

Stimulated Raman Spectroscopy with Entangled Light; Enhanced Resolution and Pathway Selection

Konstantin E. Dorfman,* Frank Schlawin, and Shaul Mukamel

Department of Chemistry, University of California, Irvine, California 92697-2025, USA

E-mail: kdorfman@uci.edu

*To whom correspondence should be addressed

Abstract

We propose a novel femtosecond stimulated Raman spectroscopy (FSRS) technique that combines entangled photons with interference detection to select matter pathways and enhance the resolution. Following photo excitation by an actinic pump, the measurement uses a pair of broadband entangled photons, one (signal) interacts with the molecule together with a third narrowband pulse induces the Raman process. The other (idler) photon provides a reference for the coincidence measurement. This interferometric photon-coincidence counting detection allows to separately measure Raman gain and loss signals, which is not possible with conventional probe transmission detection. Entangled photons further provide a unique temporal and spectral detection window that can better resolve fast excited state dynamics compared to classical and correlated disentangled states of light.

Keywords: Femtosecond Raman Spectroscopy, entangled photons, interferometry

Stimulated Raman spectroscopy is one of the most versatile tools for the study of molecular vibrations. Applications include probing time-resolved photophysical and photochemical processes¹⁻⁴, chemically specific biomedical imaging⁵, and chemical sensing^{6,7}. Considerable effort has been devoted to eliminate off-resonant background thus improving the signal to noise ratio and the ability to detect small samples and even single molecules. Pulse shaping^{8,9} and the combination of broad and narrow band pulses (technique known as Femtosecond Stimulated Raman Spectroscopy (FSRS)¹) were employed. Recent measurements of absorption spectra with entangled photons in an interferometric setup¹⁰⁻¹⁴ suggest a possibility to use more elaborate detection. Here we propose an Interferometric FSRS (IFSRS) technique that combines quantum entangled light with interferometric detection to significantly enhance the resolution and selectivity of Raman signals. By counting photons, IFSRS can further measure separately the gain and loss contributions to the Raman spectra¹⁵ which is not possible with classical FSRS.

Entangled light is widely used in quantum information^{16,17}, secure communication¹⁸ and quantum computing¹⁹ applications. It has been demonstrated that the twin photon state may be used to manipulate two photon absorption $\omega_1 + \omega_2$ type resonances in aggregates²⁰⁻²³ but these ideas do not apply to Raman $\omega_1 - \omega_2$ resonances. We show that this can be achieved by using interferometric photon coincidence detection, which further enhances the signal-to-noise ratio. Moreover, entangled two-photon absorption has also been shown experimentally to scale linearly rather than quadratically with the pump intensity^{21,24} thus allowing to use very weak light intensities, limiting damage and overcoming the photodetector noise when employing the photon coincidence measurement²⁵.

In conventional FSRS, an actinic resonant pulse \mathcal{E}_a first creates a vibrational wave packet in an electronically excited state (see 1a,b). After a delay T , the frequency resolved transmission of a broadband (femtosecond) probe E_s in the presence of a narrowband (picosecond) pump \mathcal{E}_p shows excited state vibrational resonances generated by an off-resonant stimulated Raman process. The

FSRS signal is given by²⁶

$$S_{FSRS}(\omega, T) = \frac{2}{\hbar} \mathcal{I} \int_{-\infty}^{\infty} dt e^{i\omega(t-T)} \mathcal{T} \mathcal{E}_s^*(\omega) \mathcal{E}_p(t) \langle \alpha(t) e^{-\frac{i}{\hbar} \int H'_-(\tau) d\tau} \rangle, \quad (1)$$

where α is the electronic polarizability, \mathcal{I} denotes the imaginary part, $\langle \dots \rangle = \text{tr}[\dots \rho]$ with ρ being the density operator of the entire system, and $\mathcal{E}_s = \langle E_s \rangle$ is expectation value of the probe field operator with respect to classical state of light (hereafter \mathcal{E} denotes classical fields and E stands for quantum fields). H'_- is the Hamiltonian superoperator²⁷ in the interaction picture (see Section 1 of SI). The exponent in Eq. (??) can be expanded perturbatively in field-matter interactions (see Section 2 of SI). Off-resonance Raman processes can be described by the radiation/matter interaction Hamiltonian $H'(t) = \alpha E_s^\dagger(t) \mathcal{E}_p(t) + \mathcal{E}_a^*(t) V + H.c.$, where V is the dipole moment, α is the off-resonant polarizability. In the present applications we expand the signal (??) to sixth order in the fields $\sim \mathcal{E}_s^2 \mathcal{E}_p^2 \mathcal{E}_a^2$. The resulting classical FSRS signal is given by the two diagrams in 1c which translates into Eqs. (??) - (??) of SI. All relevant matter information is contained in the two four-point correlation functions

$$F_i(t_1, t_2, t_3) = \langle V G^\dagger(t_1) \alpha G^\dagger(t_2) \alpha G(t_3) V^\dagger \rangle, \quad (2)$$

$$F_{ii}(t_1, t_2, t_3) = \langle V G^\dagger(t_1) \alpha G(t_2) \alpha G(t_3) V^\dagger \rangle, \quad (3)$$

where the retarded Green's function $G(t) = (-i/\hbar) \theta(t) e^{-iHt}$ represents forward time evolution with the free-molecule Hamiltonian H (diagrams (1,1)a, (1,1)b) and G^\dagger represents backward evolution. F_i involves one forward and two backward evolution periods while F_{ii} contains two forward followed by one backward propagation. F_i and F_{ii} differ by the final state of the matter. In F_i (F_{ii}) it is different (the same) from the state after the actinic pulse preparation.

To use entangled light in the IFSRS measurement we first generate frequency and polarization entangled photon pairs via type-II parametric down conversion (PDC)²⁸. The barium borate (BBO)

crystal pumped by a femtosecond pulse creates a pair of orthogonally polarized photons which are initially separated by a polarizing beam splitter (BS) in 1d and then directed into two arms of the Hanbury-Brown-Twiss interferometer²⁹. Horizontally polarized beam s interacts with the molecule and serves as a Raman probe in standard FSRS setup, whereas vertically polarized beam r propagates freely and provides a reference. The time-and-frequency resolved detection via ultrafast upconversion of the photons³⁰ in IFSRS provides spectroscopic information about excited state vibrational dynamics of the molecule in the s arm. IFSRS has the following control parameters: the time and frequency parameters of the single photon detectors, which can time the photons with up to ~ 100 fs resolution³⁰, frequency of the narrowband classical pump pulse ω_p and the time delay T between the actinic pulse \mathcal{E}_a and the probe E_s .

The photon state produced by PDC has two contributions: a vacuum state and two-photon state with single photon in the s - mode and single photon in the r - mode and is described by the wavefunction

$$|\psi\rangle = |0\rangle + \int_{-\infty}^{\infty} d\omega_s d\omega_r \Phi(\omega_s, \omega_r) a_{\omega_s}^\dagger a_{\omega_r}^\dagger |0\rangle, \quad (4)$$

where $a_{\omega_s}^\dagger$ ($a_{\omega_r}^\dagger$) is the creation operator of a horizontally (vertically) polarized photon and the two-photon amplitude $\Phi(\omega_s, \omega_r)$ is given by²²

$$\Phi(\omega_s, \omega_r) = \mathcal{E}_0(\omega_s + \omega_r) \sum_{i \neq j=1}^2 \text{sinc}(\omega_{s0} T_i / 2 + \omega_{r0} T_j / 2) e^{i\omega_{s0} T_i / 2 + i\omega_{r0} T_j / 2}, \quad (5)$$

where $\omega_{k0} = \omega_k - \omega_0$, $k = s, r$ is the frequency difference between entangled photon and the classical PDC-pump field \mathcal{E}_0 that created an entangled pair. In the following simulations we assumed a lorentzian field envelope $\mathcal{E}_0(\omega) = A_0 / [\omega - \omega_0 + i\sigma_0]$. $T_j = (1/v_p - 1/v_j)L$, $k = s, r$ is the time delay acquired by the entangled photon relative to the PDC-pump field due to group velocity dispersion inside the nonlinear crystal. $T_{12} = T_2 - T_1$ is the entanglement time, which controls the timing of the entangled pair. For a narrowband PDC-pump $\mathcal{E}_0(\omega)$ the sum-frequency $\omega_s + \omega_r$ is narrowly distributed around $2\omega_0$ with bandwidth σ_0 . This has been used to selectively prepare

double exciton states in two-photon absorption^{21,22}. For a broadband PDC-pump the frequency difference $\omega_s - \omega_0$ is narrow with bandwidth T_j^{-1} , $j = 1, 2$. The output state of light in mode s may contain a varying number of photons, depending on the order of the field-matter interaction.

In general, the twin photon state Eq. (??) is not necessarily entangled. This can be determined by the Schmidt decomposition³¹

$$\Phi(\omega_s, \omega_r) = \sum_n \sqrt{\lambda_n} \psi_n(\omega_s) \phi_n(\omega_r) \quad (6)$$

where λ_k are the real positive singular values of Φ and $\psi_n(\phi_n)$ form an orthonormal set of eigenfunctions of $\int d\omega \Phi(\omega_s, \omega) \Phi^*(\omega_r, \omega)$ ($\int d\omega \Phi(\omega, \omega_s) \Phi^*(\omega, \omega_r)$) with $\sum_n \lambda_n = 1$ for the normalized two-photon state. A separable (unentangled) state has only one non vanishing eigenvalue $\lambda_1 = 1$ whereas two or more components imply entanglement. The degree of entanglement can be measured by the inverse participation ratio $r_p \equiv (\sum_n \lambda_n^2)^{-1}$. For the two-photon amplitude in Eq. (??) the rich spectrum of eigenvalues shown in 2d indicates that the state is highly entangled as $r_p \sim 100$. In addition as can be seen from the insert in 2a,b, state (??) is not bound by the Fourier uncertainty $\Delta\omega\Delta t \geq 1$. In the following we study effects of the entanglement on Raman resonances.

The *IFSRS* is given by the rate of a joint time-and-frequency gated detection of N_s photons in detector s and a single photon in r when both detectors have narrow spectral gating. This is given by

$$S_{IFSRS}^{(N_s, 1)}(\bar{\omega}_{s_1}, \dots, \bar{\omega}_{s_{N_s}}, \bar{\omega}_r, \Gamma_i) = \langle \mathcal{T} E_r^\dagger(\bar{\omega}_r) E_r(\bar{\omega}_r) \prod_{j=1}^{N_s} E_s^\dagger(\bar{\omega}_{s_j}) E_s(\bar{\omega}_{s_j}) e^{-\frac{i}{\hbar} \int_{-\infty}^{\infty} H'_-(\tau) d\tau} \rangle. \quad (7)$$

where Γ_i represents the incoming light beams, such as central frequency and time, spectral and temporal bandwidth. In the standard Glauber's approach³² photon counting is calculated in the space of the radiation field using normally ordered field operators. Eq.(??) in contrast operates in the joint matter plus field space and uses time ordered superoperators³³. This is necessary for the bookkeeping of spectroscopic signals. Both FSRS and IFSRS signals are obtained by the lowest (sixth) order perturbative expansion of Eq. (??) in field-matter interactions (Section 2 of SI) as

depicted by the loop diagrams shown in 1c and e, respectively. Measurements with a different number of photons in the s arm are experimentally distinct and are given by different detection windows governed by multipoint correlation function of electric field (red arrows in 1e). Details of the derivations for the field correlation functions for twin entangled state of light are given in Section 3 of SI.

2 compares field spectrograms which represent the windows created by various fields. 2a depict a time-frequency Wigner function $W_s(\omega, t) = \int_{-\infty}^{\infty} \frac{d\Delta}{2\pi} \mathcal{E}_s^*(\omega) \mathcal{E}_s(\omega + \Delta) e^{-i\Delta t}$ for the classical probe field \mathcal{E}_s . The time-frequency Fourier uncertainty restricts the frequency resolution for a given time resolution so that $\Delta\omega\Delta t \geq 1$. The Wigner spectrogram $W_q(\omega, t; \bar{\omega}_r) = \int_{-\infty}^{\infty} \frac{d\Delta}{2\pi} \Phi^*(\omega, \bar{\omega}_r) \Phi(\omega + \Delta, \bar{\omega}_r) e^{-i\Delta t}$ for the entangled twin photon state is depicted in 2b. For the same temporal resolution as in FSRS ($\Delta\nu\Delta t \sim 3.7 \text{ ps}\cdot\text{cm}^{-1}$, which is the Fourier uncertainty for the lorentzian pulses), the spectral resolution of IFSRS is significantly better ($\Delta\nu\Delta t \sim 1.6 \text{ ps}\cdot\text{cm}^{-1}$). This is possible since the time and frequency resolution for entangled light are not Fourier conjugate variables²². The high spectral resolution in the entangled case is governed by T_j^{-1} , $j = 1, 2$ which is narrower than the broadband probe pulse. 2c demonstrates that the entangled window function $R_q^{(N_s, 1)}$ for $N_s = 1, 2$ (see Eqs. (??), (??)) that enters the IFSRS (??) yields a much higher spectral resolution than the classical R_c in Eq. (??).

The molecular information required by the Raman measurements considered here is given by two correlation functions F_i and F_{ii} (see 1c,e and Eqs. (??) - (??)). These are convoluted with a different detection window for FSRS and IFSRS. F_i and F_{ii} may not be separately detected in FSRS. However in IFSRS the loss $S_{IFSRS}^{(0,1)}$ and the gain $S_{IFSRS}^{(2,1)}$ Raman signals probe F_i where the final state c can be different from initial state a . On the other hand the coincidence counting $S_{IFSRS}^{(1,1)}$ signal is related to F_{ii} (both initial and final states are the same a). Interferometric signals can thus separately detect F_i and F_{ii} .

IFSRS for a vibrational mode in a tunneling system. We had demonstrated the combined effect of entanglement and interferometric measurement by calculating the signals for the three-level model system undergoing relaxation as depicted in 1a. Once excited by the optical pulse, the

vibrational state of the excited electronic state at initial time has frequency $\omega_{a+} = \omega_a + \delta$. For a longer time the system tunnels through a barrier at a rate k and assumes a different frequency $\omega_{a-} = \omega_a - \delta$. The probability to be in the state with ω_{a+} decreases exponentially $P_+(t) = e^{-kt}$ whereas for ω_{a-} it grows as $P_-(t) = 1 - e^{-kt}$. This model is mathematically identical to the low temperature limit of Kubo's two-state jump model described by the Stochastic Liouville Equation (SLE)^{34,35}. The absorption lineshape is given by

$$S_l(\omega) = -\mathcal{I} \frac{4}{\hbar^2} |\mathcal{E}(\omega)|^2 \frac{|\mu_{ag}|^2}{k + 2i\delta} \left(\frac{k + i\delta}{\omega - \omega_{a-} + i\gamma_a} + \frac{i\delta}{\omega - \omega_{a+} + i(\gamma_a + k)} \right). \quad (8)$$

This gives two peaks with combined width governed by dephasing γ_a and tunneling rate k . Similarly one can derive the corresponding IFSRS signal $S_{IFSRS}^{(N_s,1)}$ with $N_s = 0, 1, 2$ using SLE (see Section 4 of SI) which yields

$$\begin{aligned} S_{IFSRS}^{(N_s,1)}(\bar{\omega}_s, \bar{\omega}_r; \omega_p, T) &= \mathcal{I} \frac{\mu}{\hbar^4} |\mathcal{E}_p|^2 |\mathcal{E}_a|^2 \sum_{a,c} \alpha_{ac}^2 |\mu_{ag}|^2 \\ &\times e^{-2\gamma_a T} \left(R_q^{(N_s,1)}(\bar{\omega}_s, \bar{\omega}_r, 2\gamma_a, \bar{\nu}\omega_\nu - i\gamma_a) - \frac{2i\delta e^{-kT}}{k + 2i\delta} \right. \\ &\times [R_q^{(N_s,1)}(\bar{\omega}_s, \bar{\omega}_r, 2\gamma_a + k, \bar{\nu}\omega_\nu - i\gamma_a) \\ &\left. - R_q^{(N_s,1)}(\bar{\omega}_s, \bar{\omega}_r, 2\gamma_a + k, \bar{\nu}\omega_\nu - i(\gamma_a + k))] \right), \quad (9) \end{aligned}$$

where $\nu = -$ for $N_s = 0, 2$ and $\nu = +$ for $N_s = 1$, $\mu = -$ for $N_s = 1, 2$ and $\mu = +$ for $N_s = 0$. Expressions for the Raman response $R_q^{(N_s,1)}$ which depends on the window created by the quantum field for different photon numbers N_s are given by Eqs. (??), (??), and (??) of SI. The classical FSRS signal (??) is given by the similar expression, i.e. $S_{FSRS}^{(c)} = S_{IFSRS}^{(2,1)}[\omega_\pm] - S_{IFSRS}^{(2,1)}[-\omega_\mp]$ by replacing the entangled detection window $\Phi^*(\omega, \bar{\omega}_r)\Phi(\omega + i\gamma, \bar{\omega}_r)$ with a classical one $\mathcal{E}_s^*(\omega)\mathcal{E}_s(\omega + i\gamma_a)$.

3 compares the classical FSRS signal (Eq. (??)) with $S_{IFSRS}^{(1,1)}$ and $S_{IFSRS}^{(2,1)}$ (Eq. (??)). For slow modulation and long dephasing time $k, \gamma_a \ll \delta$ the absorption (3a) has two well-resolved peaks at ω_\pm . The classical FSRS shown in 3c then has one dominant resonance at ω_+ which

decays with the delay T , whereas the ω_- peak slowly builds up and dominates at longer T . This signal contains both blue- and red-shifted Raman resonances relative to the narrowband pump frequency: $\omega - \omega_p = \pm\omega_{\pm}$. If the modulation and dephasing rates are comparable to the level splitting $k, \gamma_a \sim \delta$, then the ω_{\pm} resonances in the absorption (3b) and the classical FSRS (3d) become broad and less resolved. It is worth noting, that there is no mirror symmetry between blue- and red- contributions around $\omega = \omega_p$. For $\omega > \omega_p$ the vibration probed by a Raman sequence of pulses at initial time has frequency $\omega - \omega_p = \omega_+ \equiv \omega_{ac} + \delta$ which gets depopulated with time whereas the transition $\omega - \omega_p = \omega_- = \omega_{ac} - \delta$ gets populated. In the case of $\omega < \omega_p$, the higher vibrational state is given by $-\omega_-$ and the lower vibrational state is $-\omega_+$. So the actual symmetry applies to $\omega_{\pm} \leftrightarrow -\omega_{\mp}$.

We next turn to IFSRS. For slow tunneling and long dephasing, $S_{IFSRS}^{(1,1)}$ is similar to the classical FSRS as shown in 3e. However both temporal and spectral resolutions remain high even when the modulation is fast and the dephasing width is large, as is seen in 3f. The same applies to the $S_{IFSRS}^{(2,1)}$ signal depicted for slow tunneling - 3g and fast tunneling - 3h. Note, that high resolution for $S_{IFSRS}^{(1,1)}$ and $S_{IFSRS}^{(2,1)}$ signals is achieved for different parameter regimes. At fixed $T_2 = 120$ fs $S_{IFSRS}^{(1,1)}$ has high resolution at short $T_1 = 10$ fs whereas long $T_1 = 110$ fs works better for $S_{IFSRS}^{(2,1)}$. This difference may be attributed to the selection of field-matter pathways by the different detection windows of the two signals. Another important difference between the long and short dephasing (top and bottom row in Fig. 3, respectively) is the overall time scale. It follows from Eqs. (??) and (??) that the signals decay exponentially with the dephasing rate $\sim e^{-2\gamma_a T}$. Therefore for a given range of $0 < T < 1.3$ ps, the signals with long dephasing (panels c,e, and g in Fig. 3) are stronger than the signals with fast dephasing (panels d,f, and g in Fig. 3).

Apart from the different detection windows, there is another important distinction between IFSRS (Eq. (??)) and FSRS (??) signals. In FSRS, the gain and loss contributions both contain red- and blue- shifted features relative to the narrow pump. The FSRS signal can contain both Stokes and anti Stokes components. Classical FSRS can only distinguish between red and blue contributions. The counting signals, in contrast, can measure separately the gain $S_{IFSRS}^{(2,1)}$ and the loss

contributions $S_{IFSRS}^{(0,1)}$ since these are not related to the classical causal response function, which is a specific combination of the quantum matter pathways. Each IFSRS signal is a different combination of pathways that can be expressed uniquely in terms of the left- and right- superoperators.

Role of entanglement. We now show that entanglement is essential for the improved resolution of Raman resonances which may not be achieved by classically shaped light. To that end we calculate the IFSRS signals (??) for the correlated-separable state of the field³⁶ described by the density matrix $\rho_{cor} = \int_{-\infty}^{\infty} d\omega_s d\omega_r |\Phi(\omega_s, \omega_r)|^2 |1_{\omega_s}, 1_{\omega_r}\rangle \langle 1_{\omega_s}, 1_{\omega_r}|$. This is the diagonal part of the density matrix corresponding to state (??) with amplitude (??). This state is not entangled but yields the same single-photon spectrum and shows strong frequency correlations similar to entangled case, and is typically used as a benchmark to quantify entanglement in quantum information processing³¹. We further examine the fully separable uncorrelated Fock state given by Eq. (??) with $\Phi_{uncor}(\omega_s, \omega_r) = \Phi_s(\omega_s)\Phi_r(\omega_r)$ with $\Phi_k(\omega_k) = \Phi_0/[\omega_k - \omega_0 + i\sigma_0]$, $k = s, r$ with parameters matching the classical probe pulse used in FSRS.

$S_{IFSRS}^{(1,1)}$ for these three states of light are compared in the left column of 4. 4a shows highly resolved Raman resonances for entangled twin state. The separable correlated state (see 4b) has high spectral but no temporal resolution, as expected from a cw time-averaged state in which the photons arrive at any time³⁶. The separable uncorrelated state (see 4c) yields the same resolution as the classical FSRS signal in 3d since the correlation function of the field factorizes into a product of field amplitudes. Similar results can be obtained for the $S_{IFSRS}^{(2,1)}$ (see 4d, e, and f respectively) Derivations of the IFSRS signals for the correlated and uncorrelated separable states are given in Section 5 of SI.

In summary, we have demonstrated that stimulated Raman signals with quantum field and interferometric detection better reveal detailed molecular information which is not possible by the standard heterodyne detection of classical fields.

Theoretical methods

In order to use quantum light as a spectroscopic tool for studying complex models of matter, the field-matter interactions must be described in the joint field and matter space. This is done

using the superoperator loop diagram formalism³⁷. Order by order in field/matter interaction, the signals can be factorized into products of field and matter time-ordered superoperator correlation functions.

The leading third order signal is governed by a four-point correlation function of the matter. Depending on number of detected photons this four-point matter correlation function is convoluted with different field correlation function. For $N_s = 0$, $N_r = 1$ Eq. (??) is given by four-point correlation function for a quantum field. For a twin photon state it can be factorized as $\langle \psi | E_s^\dagger(\omega_a) E_r^\dagger(\omega_b) E_r(\omega_c) E_s(\omega_d) | \psi \rangle = \Phi^*(\omega_a, \omega_b) \Phi(\omega_c, \omega_d)$. For $N_s = 2$ it is given by eight-point (see Eq. (??)), whereas for $N_s = 1$ it is governed by a six-point field correlation function as shown in Eqs. (??) - (??). For the two-photon state, normally-ordered field correlation functions with more than 4 fields vanish since extra annihilation operators act on the vacuum state. Therefore, the higher order non-normally ordered field correlation functions can be recast as a four-point correlation function times multiple field commutators, which are given by $[E_s(\omega), E_s^\dagger(\omega')] = \mathcal{D}(\omega_p) \delta(\omega - \omega')$ where $\mathcal{D}(\omega_s) \simeq \mathcal{D}(\omega_p)$ is the constant which is assumed to be a flat function of its argument for a normalized two photon state. Therefore for $N_s = 2$ and $N_s = 1$ the signal is proportional to $\mathcal{D}^2(\omega_p)$ and $\mathcal{D}(\omega_p)$, respectively. All three IFSRS signals with $N_s = 0, 1, 2$ scale as $\sim |\mathcal{E}_0|^2 |\mathcal{E}_a|^2 |\mathcal{E}_p|^2$ with field intensity, the same as classical FSRS even though a different number of fields contribute to the detection.

Acknowledgements

We gratefully acknowledge the support of the National Science Foundation through Grant No. CHE-1058791 and computations are supported by CHE-0840513, the Chemical Sciences, Geosciences and Biosciences Division, Office of Basic Energy Sciences, Office of Science and US Department of Energy, National Institute of Health Grant No. GM-59230. F.S. would like to thank the German National Academic Foundation.

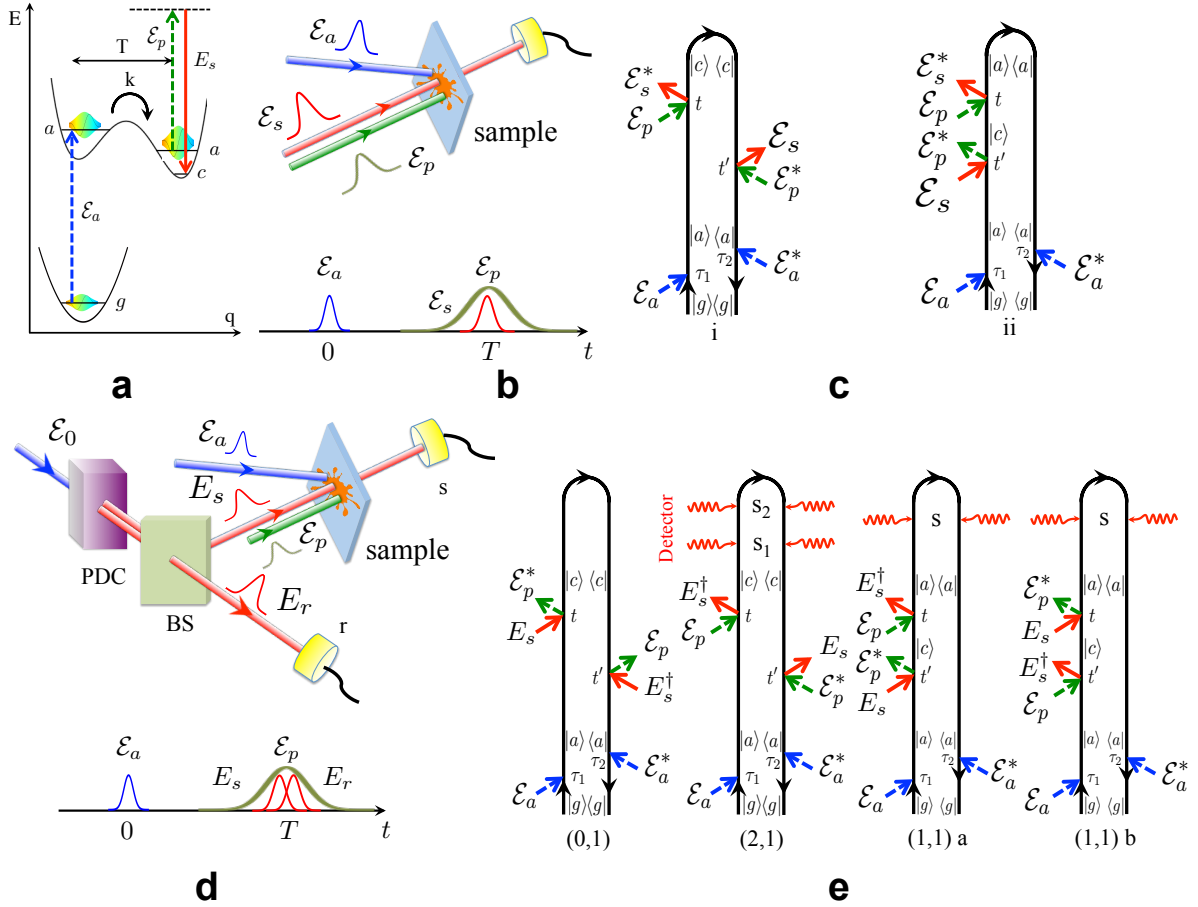


Figure 1: (Color online) Top row: classical FSRs level scheme for the tunneling model - **a**, pulse configuration - **b**, and loop diagrams (for diagram rules see³⁷) for classical FSRs - **c**. **d** and **e** - the same as **b**, and **c** but for IFSRS. BS and PDC in **d** are the beam splitter and parametric down conversion, respectively. The pairs of indices $(0, 1)$ etc. in **e** indicate number of photons registered by detectors s and r in each photon counting signal: (N_s, N_r)

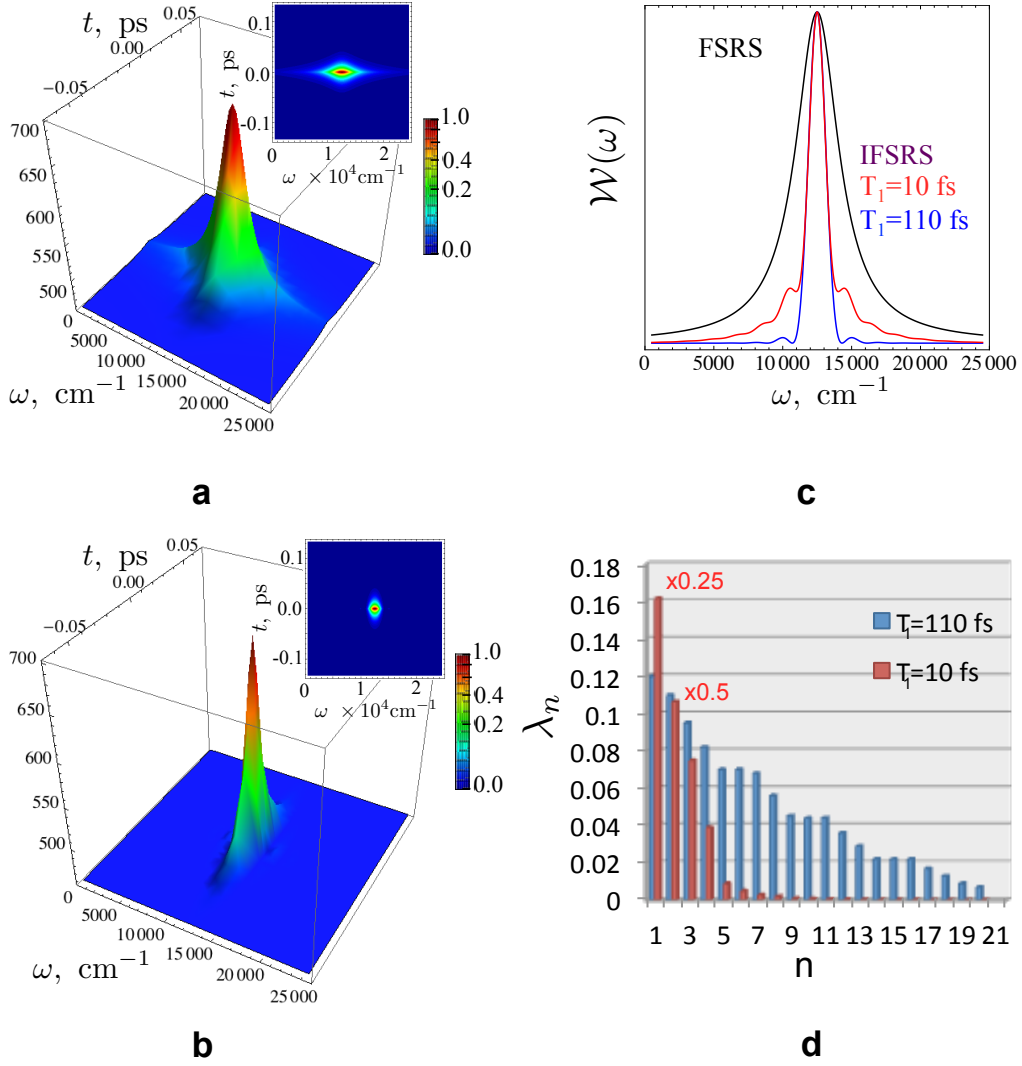


Figure 2: (Color online) Left column: **a** - time-frequency Wigner spectrogram for classical light, **b** - same as **a** but for entangled twin state given by Eq. (??). Inserts depict a 2D projection. Right column: **c** - window function for FRS $\mathcal{E}_s^*(\omega)\mathcal{E}_s(\omega + i\gamma_a)$ -black, and IFSRS $\Phi^*(\omega, \bar{\omega}_r)\Phi(\omega + i\gamma_a, \bar{\omega}_r)$ with $T_1 = 110$ fs, $T_2 = 120$ fs, and $T_1 = 10$ fs, $T_2 = 120$ fs - red. **d** - spectrum of the eigenvalues λ_n in the Schmidt decomposition (??) for entangled state with amplitude (??). The first two eigenvalues $n = 1, 2$ are scaled with weights 0.25, 0.5, respectively. The remaining eigenvalues have no weighted scaling.

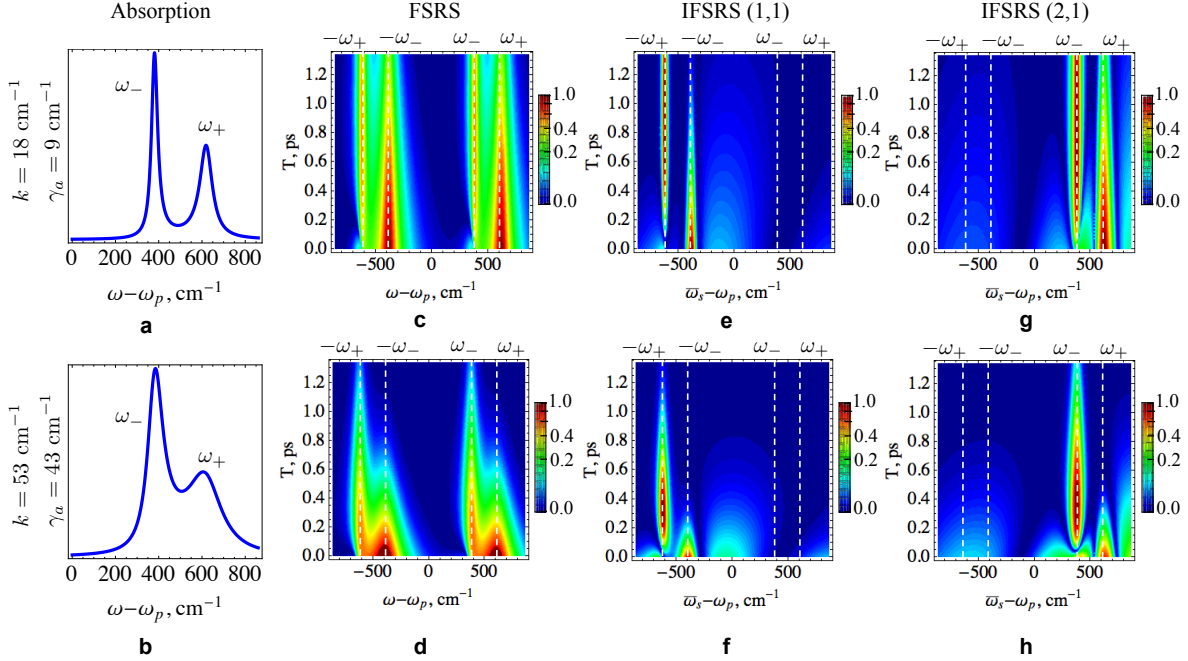


Figure 3: (Color online) First column: **a** - Absorption for a time evolving vibrational mode i vs $\omega - \omega_p$ for slow tunneling rate $k = 18 \text{ cm}^{-1}$ and narrow dephasing $\gamma_a = 9 \text{ cm}^{-1}$, **b** - same as **a** but for fast tunneling rate $k = 53 \text{ cm}^{-1}$ and broad dephasing $\gamma_a = 43 \text{ cm}^{-1}$. Second column: **c**, **d** - same as **a**, **b** but for classical FRS signal. Third column: **e** and **f** - same as **a**, **b** but for $S_{IFRS}^{(1,1)}$. Fourth column: **g**, **h** - same as **a**, **b** but for $S_{IFRS}^{(2,1)}$ given by Eq. (??) vs $\bar{\omega}_s - \omega_p$. Parameters for the simulations: unperturbed vibration frequency $\omega_{ac} = 500 \text{ cm}^{-1}$, level splitting $\delta = 120 \text{ cm}^{-1}$, $\omega_p = 12500 \text{ cm}^{-1}$, $\bar{\omega}_r = 15500 \text{ cm}^{-1}$, and $T_2 = 120 \text{ fs}$. $T_1 = 10 \text{ fs}$ for **c**, **d** and $T_1 = 110 \text{ fs}$ for **e** and **f**. The series of the snapshots (slices of panels **c-h**) are shown in 5 of SI.

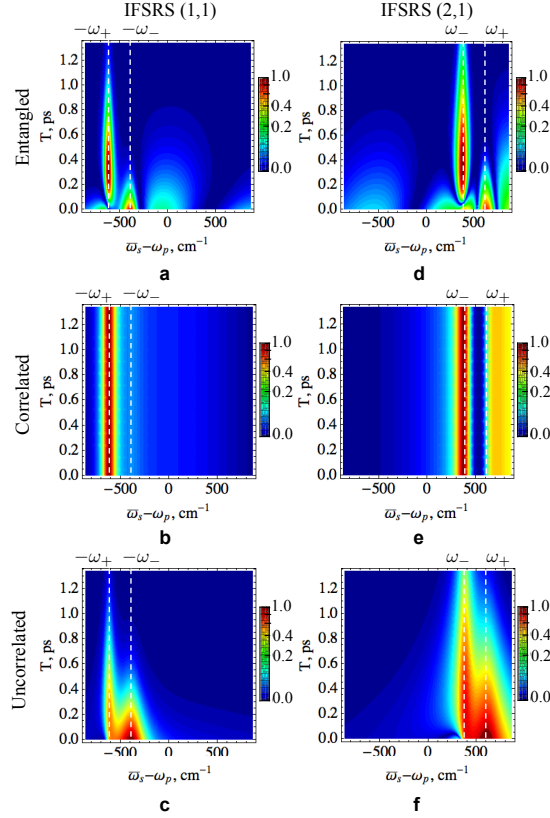


Figure 4: (Color online) Left column: $S_{IFSRS}^{(1,1)}$ signal vs $\bar{\omega}_s - \omega_p$ for entangled state (??) - **a**, correlated - **b** and uncorrelated - **c** separable states. **d**, **e**, and **f** - same as **a**, **b**, and **c** but for $S_{IFSRS}^{(2,1)}$ signal. All parameters are the same as in 3. The corresponding series of the snapshots (slices of these plots) are shown in 6 of SI.

SUPPLEMENTARY INFORMATION:
**Stimulated Raman Spectroscopy with Entangled Light; Enhanced
Resolution and Pathway Selection**

1 Time-and-frequency resolved photon counting signals

The joint time-and-frequency gated rate of detecting N_s photons in detector s and N_r in r is formally given by³⁸

$$S_{IS}^{(N_s, N_r)}(\Gamma_{s_1}, \dots, \Gamma_{s_{N_s}}, \Gamma_{r_1}, \dots, \Gamma_{r_{N_r}}; \Gamma_i) = \int_{-\infty}^{\infty} dt_{s_1} \dots \int_{-\infty}^{\infty} dt_{s_{N_s}} \int_{-\infty}^{\infty} dt_{r_1} \dots \int_{-\infty}^{\infty} dt_{r_{N_r}} \\ \times \langle \mathcal{T} \prod_{k=1}^{N_r} E_{rR}^{(tf)\dagger}(t_{r_k}) E_{rL}^{(tf)}(t_{r_k}) \prod_{j=1}^{N_s} E_{sR}^{(tf)\dagger}(t_{s_j}) E_{sL}^{(tf)}(t_{s_j}) e^{-\frac{i}{\hbar} \int_{-\infty}^{\infty} H'_-(\tau) d\tau} \rangle, \quad (10)$$

where $\Gamma_{s_j}, \Gamma_{r_k}, j = 1, \dots, N_s, k = 1, \dots, N_r$ denote the set of parameters that characterize the various photons detected in s and r , and Γ_i represents the incoming light beams. In the following we only consider measurements with a single reference photon $N_r = 1$. In Eq. (??) $\langle \dots \rangle = \text{tr}[\dots \rho]$ with ρ being the density operator of the entire system, and H'_- is the Hamiltonian superoperator in the interaction picture. Superoperators provide a convenient bookkeeping of time-ordered Green's functions. With every ordinary operator A we associate two superoperators²⁷ defined by their action on an ordinary operator X as $A_L = AX$ acting from left, $A_R = XA$ (right). We further define the symmetric and antisymmetric combinations $A_+ = \frac{1}{2}(A_L + A_R)$, $A_- = A_L - A_R$, \mathcal{T} denotes superoperator time ordering.

The coincidence signal Eq. (??) depends on the time-and-frequency gated electric field $E^{(tf)}$. The detector with input located at r_D is represented by a time gate F_t centered at \bar{t} followed by a frequency gate F_f centered at $\bar{\omega}$ ³⁹. The gated field can be written as

$$E_j^{(tf)}(\bar{t}, \bar{\omega}; t) = \int_{-\infty}^{\infty} dt' F_f^{(j)}(t - t', \bar{\omega}) F_t^{(j)}(t', \bar{t}) E_j(t'). \quad (11)$$

The parameters of the time F_t and frequency F_f gates can be varied independently. However the combined temporal and spectral resolution for the signal (??) always satisfies Fourier uncertainty $\Delta\omega\Delta t \geq 1$ ³³.

Hereafter we consider two types of signals. The first has a sharp time gate $F_t^{(s_j)}(\bar{t}_{s_j}, t'_{s_j}) = \delta(t'_{s_j} - \bar{t}_{s_j})$, $j = 1, \dots, N_s$ for the s detector and narrow frequency gate for the r detector $F_f^{(r)}(\bar{\omega}_r; \omega'_r) = \delta(\omega'_r - \bar{\omega}_r)$. The signal (??) then reads

$$S_{IS}^{(N_s, 1)}(\bar{t}_{s_1}, \dots, \bar{t}_{s_{N_s}}, \bar{\omega}_r, \Gamma_i) = \langle \mathcal{I} E_r^\dagger(\bar{\omega}_r) E_r(\bar{\omega}_r) \prod_{j=1}^{N_s} E_s^\dagger(\bar{t}_{s_j}) E_s(\bar{t}_{s_j}) e^{-\frac{i}{\hbar} \int_{-\infty}^{\infty} H'_-(\tau) d\tau} \rangle, \quad (12)$$

where $\bar{t}_{s_1} < \bar{t}_{s_2} < \dots < \bar{t}_{s_{N_s}}$.

The second type of signal is obtained by replacing the time gate for detector s by the frequency gate $F_f^{(s_j)}(\bar{\omega}_{s_j}; \omega'_{s_j}) = \delta(\omega'_{s_j} - \bar{\omega}_{s_j})$, $j = 1, \dots, N_s$, retaining the same narrow frequency gate for detector r . Eq. (??) then follows from (??).

2 Femtosecond Stimulated Raman Signals

2.1 FSRS

The stimulated FSRS signal obtained in the setup shown in Fig. 1b with frequency dispersed detection of the probe is given by

$$S_{FSRS}(\omega, T) = \frac{2}{\hbar} \mathcal{I} \int_{-\infty}^{\infty} dt e^{i\omega(t-T)} \langle \mathcal{E}_s^*(\omega) \mathcal{E}_p(t) \alpha(t) e^{-\frac{i}{\hbar} \int H'_-(\tau) d\tau} \rangle, \quad (13)$$

where \mathcal{I} denotes the imaginary part and $\mathcal{E}_s = \langle E_s \rangle$ is expectation value of the probe field operator with respect to classical state of light. We next expand the signal (??) to sixth order $\sim \mathcal{E}_s^2 \mathcal{E}_p^2 \mathcal{E}_a^2$. Thus, the classical FSRS signal illustrated by the two diagrams shown in Fig. 1c is given by

$S_{FSRS}^{(c)}(\omega, T) = S_{FSRS}^{(i)}(\omega, T) + S_{FSRS}^{(ii)}(\omega, T)$ where

$$S_{FSRS}^{(i)}(\omega, T) = \frac{2}{\hbar} \mathcal{I} \int_{-\infty}^{\infty} dt e^{i\omega(t-T)} \int_{-\infty}^t d\tau_1 \int_{-\infty}^t dt' \int_{-\infty}^{t'} d\tau_2 \mathcal{E}_p(t) \mathcal{E}_p^*(t') \mathcal{E}_a^*(\tau_2) \mathcal{E}_a(\tau_1) \\ \times \mathcal{E}_s^*(\omega) \mathcal{E}_s(t') F_i(t' - \tau_2, t - t', t - \tau_1), \quad (14)$$

$$S_{FSRS}^{(ii)}(\omega, T) = \frac{2}{\hbar} \mathcal{I} \int_{-\infty}^{\infty} dt e^{i\omega(t-T)} \int_{-\infty}^t d\tau_2 \int_{-\infty}^t dt' \int_{-\infty}^{t'} d\tau_1 \mathcal{E}_p(t) \mathcal{E}_p^*(t') \mathcal{E}_a(\tau_1) \mathcal{E}_a^*(\tau_2) \\ \times \mathcal{E}_s^*(\omega) \mathcal{E}_s(t') F_{ii}(t - \tau_2, t - t', t' - \tau_1). \quad (15)$$

2.2 IFSRS

Expansion of Eq. (??) for the field matter interactions depicted by loop diagrams in Fig. 1e yields for $N_s = 0$ - Raman loss (no photon in the molecular arm)

$$S_{IFSRS}^{(0,1)}(\bar{\omega}_r; T) = \mathcal{I} \frac{1}{\hbar} \int_{-\infty}^{\infty} dt \int_{-\infty}^{\infty} dt' \int_{-\infty}^t d\tau_1 \int_{-\infty}^{t'} d\tau_2 \mathcal{E}_p(t') \mathcal{E}_p^*(t) \mathcal{E}_a(\tau_1) \mathcal{E}_a^*(\tau_2) \\ \times \langle \mathcal{T} E_s^\dagger(t') \tilde{E}_r^\dagger(\bar{\omega}_r) \tilde{E}_r(\bar{\omega}_r) E_s(t) \rangle F_i(t' - \tau_2, t - t', t - \tau_1). \quad (16)$$

To make sure that there is no photon at detector s we had integrated over its full bandwidth, thus eliminating the dependence on detector parameters. For the Raman gain $N_s = 2$ signal we get

$$S_{IFSRS}^{(2,1)}(\bar{t}_{s1}, \bar{t}_{s2}, \bar{\omega}_r; T) = \mathcal{I} \frac{1}{\hbar} \int_{-\infty}^{\bar{t}_{s1}} dt \int_{-\infty}^{\bar{t}_{s1}} dt' \int_{-\infty}^t d\tau_1 \int_{-\infty}^{t'} d\tau_2 \mathcal{E}_p(t) \mathcal{E}_p^*(t') \mathcal{E}_a(\tau_1) \mathcal{E}_a^*(\tau_2) \\ \times \langle \mathcal{T} E_s(t') \tilde{E}_s^\dagger(\bar{t}_{s1}) \tilde{E}_s^\dagger(\bar{t}_{s2}) \tilde{E}_r^\dagger(\bar{\omega}_r) \tilde{E}_r(\bar{\omega}_r) \tilde{E}_s(\bar{t}_{s2}) \tilde{E}_s(\bar{t}_{s1}) E_s^\dagger(t) \rangle F_i(t' - \tau_2, t - t', t - \tau_1). \quad (17)$$

Similarly for $N_s = 1$ we obtain

$$S_{IFSRS}^{(1,1)a}(\bar{t}_s, \bar{\omega}_r; T) = -\mathcal{I} \frac{1}{\hbar} \int_{-\infty}^{\bar{t}_s} dt \int_{-\infty}^t dt' \int_{-\infty}^{t'} d\tau_1 \int_{-\infty}^{\bar{t}_s} d\tau_2 \mathcal{E}_p(t) \mathcal{E}_p^*(t') \mathcal{E}_a(\tau_1) \mathcal{E}_a^*(\tau_2) \\ \times \langle \mathcal{T} \tilde{E}_s^\dagger(\bar{t}_s) \tilde{E}_r^\dagger(\bar{\omega}_r) \tilde{E}_r(\bar{\omega}_r) \tilde{E}_s(\bar{t}_s) E_s^\dagger(t) E_s(t') \rangle F_{ii}(t - \tau_2, t - t', t' - \tau_1), \quad (18)$$

$$\begin{aligned}
S_{IFSRs}^{(1,1)b}(\bar{t}_s, \bar{\omega}_r; T) &= -\mathcal{I} \frac{1}{\hbar} \int_{-\infty}^{\bar{t}_s} dt \int_{-\infty}^t dt' \int_{-\infty}^{t'} d\tau_1 \int_{-\infty}^{\bar{t}_s} d\tau_2 \mathcal{E}_p(t') \mathcal{E}_p^*(t) \mathcal{E}_a(\tau_1) \mathcal{E}_a^*(\tau_2) \\
&\times \langle \mathcal{I} \tilde{E}_s^\dagger(\bar{t}_s) \tilde{E}_r^\dagger(\bar{\omega}_r) \tilde{E}_r(\bar{\omega}_r) \tilde{E}_s(\bar{t}_s) E_s(t) E_s^\dagger(t') \rangle F_{ii}(t - \tau_2, t - t', t' - \tau_1), \quad (19)
\end{aligned}$$

where $\tilde{E} = E^{t'f}$ is the gated field and \mathcal{R} denotes the real part that comes from the complex conjugate diagrams shown in Fig. 1e.

One can similarly express the signal (??) with $N_s = 2$ when both s and r detectors have narrow frequency gates

$$\begin{aligned}
S_{IFSRs}^{(2,1)}(\bar{\omega}_{s_1}, \bar{\omega}_{s_2}, \bar{\omega}_r; T) &= \mathcal{I} \frac{1}{\hbar} \int_{-\infty}^{\infty} d\bar{t}_{s_1} e^{i\bar{\omega}_{s_1}(\bar{t}_{s_1} - T)} \int_{-\infty}^{\bar{t}_{s_1}} dt \int_{-\infty}^t dt' \int_{-\infty}^{t'} d\tau_1 \int_{-\infty}^{t'} d\tau_2 \mathcal{E}_p(t) \mathcal{E}_p^*(t') \mathcal{E}_a(\tau_1) \mathcal{E}_a^*(\tau_2) \\
&\times \langle \mathcal{I} E_s(t') \tilde{E}_s^\dagger(\bar{\omega}_{s_1}) \tilde{E}_s^\dagger(\bar{\omega}_{s_2}) \tilde{E}_r^\dagger(\bar{\omega}_r) \tilde{E}_r(\bar{\omega}_r) \tilde{E}_s(\bar{\omega}_{s_2}) \tilde{E}_s(\bar{t}_{s_1}) E_s^\dagger(t) \rangle F_{ii}(t' - \tau_2, t - t', t - \tau_1). \quad (20)
\end{aligned}$$

Similarly the $N_s = 1$ signal is given by

$$\begin{aligned}
S_{IFSRs}^{(1,1)a}(\bar{\omega}_s, \bar{\omega}_r; T) &= -\mathcal{I} \frac{1}{\hbar} \int_{-\infty}^{\infty} dt'_s e^{i\bar{\omega}_s(t'_s - T)} \int_{-\infty}^{t'_s} dt \int_{-\infty}^t dt' \int_{-\infty}^{t'} d\tau_1 \int_{-\infty}^{t'_s} d\tau_2 \mathcal{E}_p(t) \mathcal{E}_p^*(t') \mathcal{E}_a(\tau_1) \mathcal{E}_a^*(\tau_2) \\
&\times \langle \mathcal{I} \tilde{E}_s^\dagger(\bar{\omega}_s) \tilde{E}_r^\dagger(\bar{\omega}_r) \tilde{E}_r(\bar{\omega}_r) \tilde{E}_s(t'_s) E_s^\dagger(t) E_s(t') \rangle F_{ii}(t - \tau_2, t - t', t' - \tau_1), \quad (21)
\end{aligned}$$

$$\begin{aligned}
S_{IFSRs}^{(1,1)b}(\bar{\omega}_s, \bar{\omega}_r; T) &= -\mathcal{I} \frac{1}{\hbar} \int_{-\infty}^{\infty} dt'_s e^{i\bar{\omega}_s(t'_s - T)} \int_{-\infty}^{t'_s} dt \int_{-\infty}^t dt' \int_{-\infty}^{t'} d\tau_1 \int_{-\infty}^{t'_s} d\tau_2 \mathcal{E}_p(t') \mathcal{E}_p^*(t) \mathcal{E}_a(\tau_1) \mathcal{E}_a^*(\tau_2) \\
&\times \langle \mathcal{I} \tilde{E}_s^\dagger(\bar{\omega}_s) \tilde{E}_r^\dagger(\bar{\omega}_r) \tilde{E}_r(\bar{\omega}_r) \tilde{E}_s(t'_s) E_s(t) E_s^\dagger(t') \rangle F_{ii}(t - \tau_2, t - t', t' - \tau_1). \quad (22)
\end{aligned}$$

3 Field correlation functions of entangled light for various IF-SRS signals

All our signals (??) - (??) involve products of multiple fields and four point correlation functions of matter. For $N_s = 0$, $N_r = 1$ the four-point correlation function in Eq. (??) for a quantum field in

a twin photon state can be factorized as

$$\langle \psi | E_s^\dagger(t') \tilde{E}_r^\dagger(\bar{\omega}_r) \tilde{E}_r(\bar{\omega}_r) E_s(t) | \psi \rangle = \langle \psi | E_s^\dagger(t') \tilde{E}_r^\dagger(\bar{\omega}_r) | 0 \rangle \langle 0 | \tilde{E}_r(\bar{\omega}_r) E_s(t) | \psi \rangle. \quad (23)$$

The twin state of light is described by the wavefunction (??). The two point correlation functions in Eq. (??) are then given by

$$\langle 0 | \tilde{E}_r(\bar{\omega}_r) E_s(t) | \psi \rangle = \Phi(t, \bar{\omega}_r) = \int_{-\infty}^{\infty} \frac{d\omega}{2\pi} e^{-i\omega t} \Phi(\omega, \bar{\omega}_r), \quad (24)$$

and

$$\langle \psi | E_s^\dagger(t') \tilde{E}_r^\dagger(\bar{\omega}_r) | 0 \rangle = \Phi^*(t', \bar{\omega}_r) = \int_{-\infty}^{\infty} \frac{d\omega'}{2\pi} e^{i\omega' t'} \Phi^*(\omega', \bar{\omega}_r), \quad (25)$$

The four point correlation function in Eq. (??) is finally given by

$$\langle \psi | E_s^\dagger(t') \tilde{E}_r^\dagger(\bar{\omega}_r) \tilde{E}_r(\bar{\omega}_r) E_s(t) | \psi \rangle = \Phi^*(t', \bar{\omega}_r) \Phi(t, \bar{\omega}_r). \quad (26)$$

We next turn to the $N_s = 2$, $N_r = 1$ signal (Eq. (??)). In order to evaluate the necessary eight-point field correlation function one can recast it in a normally ordered form (all annihilation operators are to the right of the creation operators). For a twin photon state normally ordered correlation functions of the field with more than 4 fields vanish since extra annihilation operators act on the vacuum. Therefore, the eight-point field correlation function in (??) can be recast as a four-point correlation function similar to Eq. (??) times two field commutators

$$[E_s(t), E_s^\dagger(t')] = \mathcal{D}(\omega_p) \delta(t - t'), \quad [E_s(\omega), E_s^\dagger(\omega')] = \mathcal{D}(\omega_p) \delta(\omega - \omega'), \quad (27)$$

where $\mathcal{D}(\omega_s) \simeq \mathcal{D}(\omega_p \pm \omega_{ac}) \simeq \mathcal{D}(\omega_p)$ is the normalization constant which is assumed to be a flat

function of its argument. We thus obtain

$$\begin{aligned}
& \langle \psi | E_s(t') \tilde{E}_s^\dagger(\bar{t}_{s_1}) \tilde{E}_s^\dagger(\bar{t}_{s_2}) \tilde{E}_r^\dagger(\bar{\omega}_r) \tilde{E}_r(\bar{\omega}_r) \tilde{E}_s(\bar{t}_{s_2}) \tilde{E}_s(\bar{t}_{s_1}) E_s^\dagger(t) | \psi \rangle \\
&= \mathcal{D}^2(\omega_p) [\Phi^*(\bar{t}_{s_1}, \bar{\omega}_r) \Phi(\bar{t}_{s_1}, \bar{\omega}_r) \delta(t - \bar{t}_{s_2}) \delta(t' - \bar{t}_{s_2}) \\
&+ \Phi^*(\bar{t}_{s_2}, \bar{\omega}_r) \Phi(\bar{t}_{s_2}, \bar{\omega}_r) \delta(t - \bar{t}_{s_1}) \delta(t' - \bar{t}_{s_1}) \\
&+ \Phi^*(\bar{t}_{s_1}, \bar{\omega}_r) \Phi(\bar{t}_{s_2}, \bar{\omega}_r) \delta(t - \bar{t}_{s_1}) \delta(t' - \bar{t}_{s_2}) \\
&+ \Phi^*(\bar{t}_{s_2}, \bar{\omega}_r) \Phi(\bar{t}_{s_1}, \bar{\omega}_r) \delta(t - \bar{t}_{s_2}) \delta(t' - \bar{t}_{s_1})]. \tag{28}
\end{aligned}$$

Finally we turn to the $N_s = N_r = 1$ signal (Eq. (??)) which is governed by a six-point correlation function. The only contribution to this correlation function comes from the four-point correlation function of normally ordered fields multiplied by a commutator of the field:

$$\langle \tilde{E}_s^\dagger(\bar{t}_s) \tilde{E}_r^\dagger(\bar{\omega}_r) \tilde{E}_r(\bar{\omega}_r) \tilde{E}_s(\bar{t}_s) E_s^\dagger(t) E_s(t') \rangle = \mathcal{D}(\omega_p) \Phi^*(\bar{t}_s, \bar{\omega}_r) \Phi(t', \bar{\omega}_r) \delta(t - \bar{t}_s). \tag{29}$$

Similarly for Eq. (??) we obtain

$$\begin{aligned}
\langle \tilde{E}_s^\dagger(\bar{t}_s) \tilde{E}_r^\dagger(\bar{\omega}_r) \tilde{E}_r(\bar{\omega}_r) \tilde{E}_s(\bar{t}_s) E_s(t) E_s^\dagger(t') \rangle &= \mathcal{D}(\omega_p) \Phi^*(\bar{t}_s, \bar{\omega}_r) \Phi(\bar{t}_s, \bar{\omega}_r) \delta(t - t') \\
&+ \mathcal{D}(\omega_p) \Phi^*(\bar{t}_s, \bar{\omega}_r) \Phi(t, \bar{\omega}_r) \delta(t' - \bar{t}_s). \tag{30}
\end{aligned}$$

It is worth noting that according to diagram (1,1)*b* in Fig. 1e, the signal (??) has $\bar{t}_s > t > t'$. However it follows from the second term in Eq. (??) that $t' = \bar{t}_s$, i.e. $t < t'$. Therefore this term does not contribute to the signal. Note also that like the classical FSRS signal all three IFSRS signals (??) - (??) scale linearly with the classical pump intensity $S_{IFSRS} \propto |A_0|^2$, even though they are governed by different number of fields contribution to the detection events.

4 Stimulated Raman signals for a vibrational tunneling model

Below we discuss a dynamical vibration model. We consider a single vibrational mode that can assume two states with frequencies $\omega_{\pm} = \omega_{ac} \pm \delta$ and a tunneling rate between them k . Following the stochastic Liouville equation approach outlined in³⁵, the absorption lineshape for such a system is given by Eq. (??).

The matter correlation functions in Eqs. (??) - (??) $F_j(t_1, t_2, t_3) \rightarrow \mathcal{F}_j(t_1 - t_2, t_2 - t_3)$, $j = i, ii$ where

$$\mathcal{F}_i(t_1, t_2) = \frac{i}{\hbar^3} \sum_{a,c} |\mu_{ag}|^2 \alpha_{ac}^2 \theta(t_1) \theta(t_2) e^{-\gamma_a(t_1+2t_2)} \left[e^{-i\omega_- t_1} - \frac{2i\delta}{k+2i\delta} e^{-kt_2} \left(e^{-i\omega_- t_1} - e^{-(k+i\omega_+)t_1} \right) \right], \quad (31)$$

$$\mathcal{F}_{ii}(t_1, t_2) = -\frac{i}{\hbar^3} \sum_{a,c} |\mu_{ag}|^2 \alpha_{ac}^2 \theta(t_1) \theta(t_2) e^{-\gamma_a(t_1+2t_2)} \left[e^{i\omega_+ t_1} - \frac{2i\delta}{k+2i\delta} e^{-kt_2} \left(e^{i\omega_+ t_1} - e^{-(k-i\omega_-)t_1} \right) \right]. \quad (32)$$

Using (??) the classical FSRS signal (??) - (??) reads

$$S_{FSRS}^{(c)}(\omega, T) = -\mathcal{I} \frac{2}{\hbar^4} |\mathcal{E}_p|^2 |\mathcal{E}_a|^2 \sum_{a,c} \alpha_{ac}^2 |\mu_{ag}|^2 e^{-2\gamma_a T} \left[R_c(\omega, 2\gamma_a, \omega_- - i\gamma_a) - \frac{2i\delta e^{-kT}}{k+2i\delta} [R_c(\omega, 2\gamma_a + k, \omega_- - i\gamma_a) - R_c(\omega, 2\gamma_a + k, \omega_+ - i(\gamma_a + k))] - (\omega_{\pm} \leftrightarrow -\omega_{\mp}) \right], \quad (33)$$

where

$$R_c(\omega, \gamma, \Omega) = \frac{\mathcal{E}_s^*(\omega) \mathcal{E}_s(\omega + i\gamma)}{\omega - \omega_p - \Omega} \quad (34)$$

is the Raman response gated by the classical field.

The IFSRS $S_{IFSRS}^{(0,1)}$ signal (??) reads

$$S_{IFSRS}^{(0,1)}(\bar{\omega}_r; \omega_p, T) = \mathcal{I} \frac{1}{\hbar^4} |\mathcal{E}_p|^2 |\mathcal{E}_a|^2 \sum_{a,c} \alpha_{ac}^2 |\mu_{ag}|^2 e^{-2\gamma_a T} \left(R_q^{(0,1)}(\bar{\omega}_s, \bar{\omega}_r, 2\gamma_a, \omega_- - i\gamma_a) - \frac{2i\delta e^{-kT}}{k + 2i\delta} [R_q^{(0,1)}(\bar{\omega}_s, \bar{\omega}_r, 2\gamma_a + k, \omega_- - i\gamma_a) - R_q^{(0,1)}(\bar{\omega}_s, \bar{\omega}_r, 2\gamma_a + k, \omega_+ - i(\gamma_a + k))] \right), \quad (35)$$

where

$$R_q^{(0,1)}(\bar{\omega}_s, \bar{\omega}_r, \gamma, \Omega) = \int_{-\infty}^{\infty} \frac{d\omega}{2\pi} \frac{\Phi^*(\omega, \bar{\omega}_r) \Phi(\omega + i\gamma, \bar{\omega}_r)}{\omega - \omega_p - \Omega} \quad (36)$$

is a Raman response gate by the quantum entangled field.

We next turn to the time-gated $S_{IFSRS}^{(2,1)}$ signal (??)

$$S_{IFSRS}^{(2,1)}(\bar{t}_{s_1}, \bar{t}_{s_2}, \bar{\omega}_r; \omega_p, T) = \mathcal{I} \frac{1}{\hbar} \mathcal{D}^2(\omega_p) |\mathcal{E}_a|^2 |\mathcal{E}_p|^2 \times \sum_{i,j=1,2} \Phi^*(\bar{t}_{s_i}, \bar{\omega}_r) \Phi(\bar{t}_{s_j}, \bar{\omega}_r) e^{-i\omega_p(t_{s_j} - t_{s_i})} \mathcal{F}_i(t_{s_j} - t_{s_i}, t_{s_i}). \quad (37)$$

The corresponding frequency-gated $S_{IFSRS}^{(2,1)}$ signal (??) is given by

$$S_{IFSRS}^{(2,1)}(\bar{\omega}_{s_1}, \bar{\omega}_{s_2}, \bar{\omega}_r; \omega_p, T) = \mathcal{I} \frac{1}{\hbar^4} \mathcal{D}^2(\omega_p) |\mathcal{E}_a|^2 |\mathcal{E}_p|^2 \sum_{a,c} |\mu_{ag}|^2 \alpha_{ac}^2 \Phi^*(\bar{\omega}_{s_1}, \bar{\omega}_r) \times \left(\Phi(\bar{\omega}_{s_1}, \bar{\omega}_r) \left[\frac{1}{2\gamma_a} \frac{1}{\bar{\omega}_{s_2} - \omega_p - \omega_- + i\gamma_a} - \frac{2i\delta}{k + 2i\delta} \frac{1}{k + 2\gamma_a} \right] + i\Phi(\bar{\omega}_{s_2}, \bar{\omega}_r) e^{i(\bar{\omega}_{s_2} - \bar{\omega}_{s_1})T} \times \left(\frac{1}{\bar{\omega}_{s_2} - \omega_p - \omega_- + i\gamma_a} - \frac{1}{\bar{\omega}_{s_2} - \omega_p - \omega_+ + i(\gamma_a + k)} \right) \right) \times \left[\frac{1}{(\bar{\omega}_{s_1} - \omega_p - \omega_- + i\gamma_a)(\bar{\omega}_{s_2} - \bar{\omega}_{s_1} - 2i\gamma_a)} - \frac{2i\delta}{k + 2i\delta} \frac{1}{\bar{\omega}_{s_2} - \bar{\omega}_{s_1} - i(2\gamma_a + k)} \right] \times \left(\frac{1}{\bar{\omega}_{s_1} - \omega_p - \omega_- + i\gamma_a} - \frac{1}{\bar{\omega}_{s_1} - \omega_p - \omega_+ + i(\gamma_a + k)} \right) \right] + (s_1 \leftrightarrow s_2). \quad (38)$$

Note, that Eq. (??) has zero time resolution as the dependence on T does not depend upon matter parameters. This is caused by two photon detection events in detector s with narrow frequency gating. To restore time resolution one can use only single detection event e.g. $\bar{\omega}_{s_1}$ and integrate

over $\bar{\omega}_{s_2}$. Neglecting the background terms that have no resonant features we obtain

$$S_{IFSRS}^{(2,1)}(\bar{\omega}_{s_1}, \bar{\omega}_r; \omega_p, T) = -\mathcal{I} \frac{1}{\hbar^4} |\mathcal{E}_p|^2 |\mathcal{E}_a|^2 \mathcal{D}^2(\omega_p) \sum_{a,c} \alpha_{ac}^2 |\mu_{ag}|^2 e^{-2\gamma_a T} \left(R_q^{(2,1)}(\bar{\omega}_s, \bar{\omega}_r, 2\gamma_a, \omega_- - i\gamma_a) \right. \\ \left. - \frac{2i\delta e^{-kT}}{k + 2i\delta} [R_q^{(2,1)}(\bar{\omega}_s, \bar{\omega}_r, 2\gamma_a + k, \omega_- - i\gamma_a) - R_q^{(2,1)}(\bar{\omega}_s, \bar{\omega}_r, 2\gamma_a + k, \omega_+ - i(\gamma_a + k))] \right), \quad (39)$$

where

$$R_q^{(2,1)}(\bar{\omega}_s, \bar{\omega}_r, \gamma, \Omega) = \frac{\Phi^*(\bar{\omega}_s, \bar{\omega}_r) \Phi(\bar{\omega}_s + i\gamma, \bar{\omega}_r)}{\bar{\omega}_s - \omega_p - \Omega}. \quad (40)$$

Finally, for the time-gated $S_{IFSRS}^{(1,1)}$ signal (??) we obtain

$$S_{IFSRS}^{(1,1)a}(\bar{t}_s, \bar{\omega}_r; \omega_p, T) = \mathcal{R} \frac{1}{\hbar^4} \mathcal{D}(\omega_p) |\mathcal{E}_a|^2 |\mathcal{E}_p|^2 \theta(\bar{t}_s - T) \sum_{a,c} |\mu_{ag}|^2 \alpha_{ac}^2 \Phi^*(\bar{t}_s, \bar{\omega}_r) e^{-2\gamma_a \bar{t}_s} \\ \times \left[\Phi(\omega_p - \omega_+ + i\gamma_a, \bar{\omega}_r) e^{[i(\omega_+ - \omega_p) + \gamma_a](\bar{t}_s - T)} - \frac{2i\delta}{k + 2i\delta} e^{-k\bar{t}_s} \right. \\ \left. \times \left(\Phi(\omega_p - \omega_+ + i(\gamma_a + k), \bar{\omega}_r) e^{[i(\omega_+ - \omega_p) + k + \gamma_a](\bar{t}_s - T)} - \Phi(\omega_p - \omega_- + i\gamma_a, \bar{\omega}_r) e^{[i(\omega_- - \omega_p) + \gamma_a](\bar{t}_s - T)} \right) \right], \quad (41)$$

where we assume a broadband entangled light and $\sigma_0 \gg \gamma_a, k$ and neglected the residues of the two photon amplitude. Similarly for (??) we obtain

$$S_{IFSRS}^{(1,1)b}(\bar{t}_s, \bar{\omega}_r; \omega_p, T) = \mathcal{R} \frac{1}{\hbar^4} \mathcal{D}(\omega_p) |\mathcal{E}_a|^2 |\mathcal{E}_p|^2 \theta(\bar{t}_s - T) \sum_{a,c} |\mu_{ag}|^2 \alpha_{ac}^2 |\Phi(\bar{t}_s, \bar{\omega}_r)|^2 \frac{1 - e^{-2\gamma_a \bar{t}_s}}{2\gamma_a}. \quad (42)$$

The frequency gated signal (??) for the TSJ model is

$$S_{IFSRS}^{(1,1)a}(\bar{\omega}_s, \bar{\omega}_r; \omega_p, T) = -\mathcal{I} \frac{1}{\hbar^4} |\mathcal{E}_p|^2 |\mathcal{E}_a|^2 \mathcal{D}(\omega_p) \sum_{a,c} \alpha_{ac}^2 |\mu_{ag}|^2 e^{-2\gamma_a T} \left(R_q^{(2,1)}(\bar{\omega}_s, \bar{\omega}_r, 2\gamma_a, -\omega_+ - i\gamma_a) \right. \\ \left. - \frac{2i\delta e^{-kT}}{k + 2i\delta} [R_q^{(2,1)}(\bar{\omega}_s, \bar{\omega}_r, 2\gamma_a + k, -\omega_+ - i\gamma_a) - R_q^{(2,1)}(\bar{\omega}_s, \bar{\omega}_r, 2\gamma_a + k, -\omega_- - i(\gamma_a + k))] \right), \quad (43)$$

where

$$R_q^{(1,1)}(\bar{\omega}_s, \bar{\omega}_r, \gamma, \Omega) = \frac{\Phi^*(\bar{\omega}_s, \bar{\omega}_r)\Phi(\omega_p + \Omega - i\gamma, \bar{\omega}_r)}{\bar{\omega}_s - \omega_p - \Omega}. \quad (44)$$

Similarly Eq. (??) gives

$$S_{IFSRS}^{(1,1)b}(\bar{\omega}_s, \bar{\omega}_r; \omega_p, T) = \mathcal{R} \frac{1}{\hbar^4} \mathcal{D}(\omega_p) |\mathcal{E}_a|^2 |\mathcal{E}_p|^2 \sum_{a,c} |\mu_{ag}|^2 \alpha_{ac}^2 \Phi^*(\bar{\omega}_s, \bar{\omega}_r) \frac{1}{2\gamma_a} \\ \times [\Phi(\bar{\omega}_s, \bar{\omega}_r) - e^{-2\gamma_a T} \Phi(\bar{\omega}_s + 2i\gamma_a, \bar{\omega}_r)]. \quad (45)$$

The latter is a background term and has no resonant features that give Raman resonances. We therefore neglect it in the simulations.

Summarizing Eqs. (??), (??), (??), and (??) we obtain Eq. (??) with gated Raman responses given by Eqs. (??), (??), (??), and (??).

5 IFSRS with separable correlated state

The general two-photon state in Eq. (??) can be described by the density matrix

$$\rho_0 = \int_{-\infty}^{\infty} d\omega_s d\omega'_s d\omega_r d\omega'_r \Phi^*(\omega'_s, \omega'_r) \Phi(\omega_s, \omega_r) |1_{\omega_s}, 1_{\omega_r}\rangle \langle 1_{\omega'_s}, 1_{\omega'_r}|. \quad (46)$$

One can further construct a different state with the same mean energy and the same single-photon spectrum, and thus would give the same single-photon transition probability. For instance if we take a diagonal part of the density matrix in Eq. (??)

$$\rho_0 = \int_{-\infty}^{\infty} d\omega_s d\omega_r |\Phi(\omega_s, \omega_r)|^2 |1_{\omega_s}, 1_{\omega_r}\rangle \langle 1_{\omega_s}, 1_{\omega_r}|, \quad (47)$$

which results from disentanglement of the entangled state. Using this density operator one can compute the four-point correlation function of the electric field that enters all IFSRS signals:

$$\langle E_s^\dagger(\omega_1)E_r^\dagger(\omega_2)E_r(\omega_3)E_s(\omega_4) \rangle = |\Phi(\omega_1, \omega_2)|^2 \delta(\omega_1 - \omega_4) \delta(\omega_2 - \omega_3). \quad (48)$$

Using Eq. (??) the $S_{IFSRS}^{(0,1)}$ signal (??) yields

$$S_{IFSRS}^{(0,1)sep}(\bar{\omega}_s, \bar{\omega}_r; \omega_p, T) = -\mathcal{I} \frac{1}{\hbar^4} |\mathcal{E}_p|^2 |\mathcal{E}_a|^2 \mathcal{D}^2(\omega_p) \delta(0) \sum_{a,c} \alpha_{ac}^2 |\mu_{ag}|^2 \int_{-\infty}^{\infty} \frac{d\omega}{2\pi} |\Phi(\omega, \bar{\omega}_r)|^2 \left(\frac{1}{2\gamma_a[\omega - \omega_- + i\gamma_a]} - \frac{2i\delta}{[k + 2i\delta][2\gamma_a + k]} \left[\frac{1}{\omega - \omega_- + i\gamma_a} - \frac{1}{\omega - \omega_+ + i(\gamma_a + k)} \right] \right). \quad (49)$$

where $\delta(0) \simeq 1/\gamma$ is a delta-function of zero argument. The $S_{IFSRS}^{(1,1)}$ signal (??) then reads

$$S_{IFSRS}^{(1,1)sep}(\bar{\omega}_s, \bar{\omega}_r; \omega_p, T) = \mathcal{I} \frac{1}{\hbar^4} |\mathcal{E}_p|^2 |\mathcal{E}_a|^2 \mathcal{D}(\omega_p) \delta(0) \sum_{a,c} \alpha_{ac}^2 |\mu_{ag}|^2 |\Phi(\bar{\omega}_s, \bar{\omega}_r)|^2 \left(\frac{1}{2\gamma_a[\bar{\omega}_s + \omega_+ + i\gamma_a]} - \frac{2i\delta}{[k + 2i\delta][2\gamma_a + k]} \left[\frac{1}{\bar{\omega}_s + \omega_+ + i\gamma_a} - \frac{1}{\bar{\omega}_s + \omega_- + i(\gamma_a + k)} \right] \right), \quad (50)$$

Similarly $S_{IFSRS}^{(2,1)}$ signal Eq. (??) becomes

$$S_{IFSRS}^{(2,1)sep}(\bar{\omega}_s, \bar{\omega}_r; \omega_p, T) = -\mathcal{I} \frac{1}{\hbar^4} |\mathcal{E}_p|^2 |\mathcal{E}_a|^2 \mathcal{D}^2(\omega_p) \delta(0) \sum_{a,c} \alpha_{ac}^2 |\mu_{ag}|^2 |\Phi(\bar{\omega}_s, \bar{\omega}_r)|^2 \left(\frac{1}{2\gamma_a[\bar{\omega}_s - \omega_- + i\gamma_a]} - \frac{2i\delta}{[k + 2i\delta][2\gamma_a + k]} \left[\frac{1}{\bar{\omega}_s - \omega_- + i\gamma_a} - \frac{1}{\bar{\omega}_s - \omega_+ + i(\gamma_a + k)} \right] \right). \quad (51)$$

References

- (1) Kukura, P.; McCamant, D. W.; Mathies, R. A. Femtosecond Stimulated Raman Spectroscopy. *Ann. Rev. Phys. Chem.* **2007**, *58*, 461–488.
- (2) Kukura, P.; McCamant, D. W.; Yoon, S.; Wandschneider, D. B.; Mathies, R. A. Structural Observation of the Primary Isomerization in Vision with Femtosecond-Stimulated Raman. *Science* **2005**, *310*, 1006–1009.
- (3) Takeuchi, S.; Ruhman, S.; Tsuneda, T.; Chiba, M.; Taketsugu, T.; Tahara, T. Spectroscopic Tracking of Structural Evolution in Ultrafast Stilbene Photoisomerization. *Science* **2008**, *322*, 1073–1077.
- (4) Kuramochi, H.; Takeuchi, S.; Tahara, T. Ultrafast Structural Evolution of Photoactive Yellow Protein Chromophore Revealed by Ultraviolet Resonance Femtosecond Stimulated Raman Spectroscopy. *J. Phys. Chem. Lett.* **2012**, *3*, 2025–2029.
- (5) Cheng, J.-x.; Volkmer, A.; Book, L. D.; Xie, X. S. Multiplex Coherent Anti-Stokes Raman Scattering Microspectroscopy and Study of Lipid Vesicles. *J. Phys. Chem. B* **2002**, *106*, 8493–8498.
- (6) Arora, R.; Petrov, G. I.; Yakovlev, V. V.; Scully, M. O. Detecting Anthrax in the Mail by Coherent Raman Microspectroscopy. *PNAS* **2012**, doi: 10.1073/pnas.1115242108.
- (7) Bremer, M. T.; Dantus, M. Standoff Explosives Trace Detection and Imaging by Selective Stimulated Raman Scattering. *Appl. Phys. Lett.* **2013**, *103*, 061119.
- (8) Oron, D.; Dudovich, N.; Yelin, D.; Silberberg, Y. Narrow-Band Coherent Anti-Stokes Raman Signals from Broad-Band Pulses. *Phys. Rev. Lett.* **2002**, *88*, 063004.
- (9) Pestov, D.; Murawski, R. K.; Ariunbold, G. O.; Wang, X.; Zhi, M.; Sokolov, A. V.; Sautenkov, V. A.; Rostovtsev, Y. V.; Dogariu, A.; Huang, Y.; Scully, M. O. Optimizing the Laser-Pulse Configuration for Coherent Raman Spectroscopy. *Science* **2007**, *316*, 265–268.

- (10) Scarcelli, G.; Valencia, A.; Gompers, S.; Shih, Y. Remote Spectral Measurement Using Entangled Photons. *Appl. Phys. Lett.* **2003**, *83*, 5560–5562.
- (11) Yabushita, A.; Kobayashi, T. Spectroscopy by Frequency-Entangled Photon Pairs. *Phys. Rev. A* **2004**, *69*, 013806.
- (12) Kalachev, A.; Kalashnikov, D.; Kalinkin, A.; Mitrofanova, T.; Shkalikov, A.; Samartsev, V. Biphoton Spectroscopy of YAG: Er³⁺ Crystal. *Las. Phys. Lett.* **2007**, *4*, 722–725.
- (13) Slattery, O.; Ma, L.; Kuo, P.; Kim, Y.-S.; Tang, X. Frequency Correlated Biphoton Spectroscopy Using Tunable Upconversion Detector. *Las. Phys. Lett.* **2013**, *10*, 075201.
- (14) Kalashnikov, D. A.; Pan, Z.; Kuznetsov, A. I.; Krivitsky, L. A. Quantum Spectroscopy of Plasmonic Nanostructures. *Phys. Rev. X* **2014**, *4*, 011049.
- (15) Harbola, U.; Umapathy, S.; Mukamel, S. Loss and Gain Signals in Broadband Stimulated-Raman Spectra: Theoretical Analysis. *Phys. Rev. A* **2013**, *88*, 011801.
- (16) Lvovsky, A. I.; Raymer, M. G. Continuous-Variable Optical Quantum-State Tomography. *Rev. Mod. Phys.* **2009**, *81*, 299.
- (17) Lee, K.C. et al. Entangling Macroscopic Diamonds at Room Temperature. *Science* **2011**, *334*, 1253–1256.
- (18) Gisin, N.; Ribordy, G.; Tittel, W.; Zbinden, H. Quantum Cryptography. *Rev. Mod. Phys.* **2002**, *74*.
- (19) Kok, P.; Munro, W. J.; Nemoto, K.; Ralph, T. C.; Dowling, J. P.; Milburn, G. Linear Optical Quantum Computing with Photonic Qubits. *Rev. Mod. Phys.* **2007**, *79*, 135.
- (20) Saleh, B. E. A.; Jost, B. M.; Fei, H.-B.; Teich, M. C. Entangled-Photon Virtual-State Spectroscopy. *Phys. Rev. Lett.* **1998**, *80*, 3483–3486.

- (21) Lee, D.-I.; Goodson, T. Entangled Photon Absorption in an Organic Porphyrin Dendrimer. *J. Phys. Chem. B* **2006**, *110*, 25582–25585.
- (22) Schlawin, F.; Dorfman, K. E.; Fingerhut, B. P.; Mukamel, S. Suppression of Population Transport and Control of Exciton Distributions by Entangled Photons. *Nat. Commun.* **2013**, *4*, 1782.
- (23) Dorfman, K. E.; Mukamel, S. Multidimensional Spectroscopy with Entangled Light: Loop vs Ladder Delay Scanning Protocols. *New J. Phys.* **2014**, *16*, 033013.
- (24) Javanainen, J.; Gould, P. L. Linear Intensity Dependence of a Two-Photon Transition Rate. *Phys. Rev. A* **1990**, *41*, 5088–5091.
- (25) Brida, G.; Genovese, M.; Gramegna, M. Twin-Photon Techniques for Photo-Detector Calibration. *Las. Phys. Lett.* **2006**, *3*, 115.
- (26) Dorfman, K. E.; Fingerhut, B. P.; Mukamel, S. Broadband Infrared and Raman Probes of Excited-State Vibrational Molecular Dynamics: Simulation Protocols Based on Loop Diagrams. *Phys. Chem. Chem. Phys.* **2013**, *15*, 12348–12359.
- (27) Harbola, U.; Mukamel, S. Superoperator Nonequilibrium Green's Function Theory of Many-Body Systems; Applications to Charge Transfer and Transport in Open Junctions. *Phys. Rep.* **2008**, *465*, 191 – 222.
- (28) Shih, Y. Entangled Biphoton Source - Property and Preparation. *Rep. Prog. Phys.* **2003**, *66*, 1009.
- (29) Brown, R. H. A Test of a New Type of Stellar Interferometer on Sirius. *Nature* **1956**, *178*, 1046–1048.
- (30) Kuzucu, O.; Wong, F. N.; Kurimura, S.; Tovstonog, S. Time-Resolved Single-Photon Detection by Femtosecond Upconversion. *Opt. Lett.* **2008**, *33*, 2257–2259.

- (31) Law, C. K.; Walmsley, I. A.; Eberly, J. H. Continuous Frequency Entanglement: Effective Finite Hilbert Space and Entropy Control. *Phys. Rev. Lett.* **2000**, *84*, 5304–5307.
- (32) Glauber, R. *Quantum Theory of Optical Coherence*; Wiley, 2007.
- (33) Dorfman, K. E.; Mukamel, S. Indistinguishability and Correlations of Photons Generated by Quantum Emitters Undergoing Spectral Diffusion. *Sci. Rep.* **2014**, *4*, 3996.
- (34) Kubo, R. Stochastic Liouville Equations. *J. Math. Phys.* **1963**, *4*, 174–183.
- (35) Dorfman, K. E.; Fingerhut, B. P.; Mukamel, S. Time-Resolved Broadband Raman Spectroscopies: A Unified Six-Wave-Mixing Representation. *J. Chem. Phys.* **2013**, *139*, 124113.
- (36) Zheng, Z.; Saldanha, P. L.; Rios Leite, J. R.; Fabre, C. Two-Photon-Two-Atom Excitation by Correlated Light States. *Phys. Rev. A* **2013**, *88*, 033822.
- (37) Rahav, S.; Mukamel, S. Ultrafast Nonlinear Optical Signals Viewed from the Molecules Perspective: Kramers-Heisenberg Transition Amplitudes vs. Susceptibilities. *Adv. At. Mol., Opt. Phys.* **2010**, *59*, 223.
- (38) Dorfman, K. E.; Mukamel, S. Nonlinear Spectroscopy with Time- and Frequency-Gated Photon Counting: A Superoperator Diagrammatic Approach. *Phys. Rev. A* **2012**, *86*, 013810.
- (39) Stolz, H. *Time-Resolved Light Scattering from Excitons*. 1994.

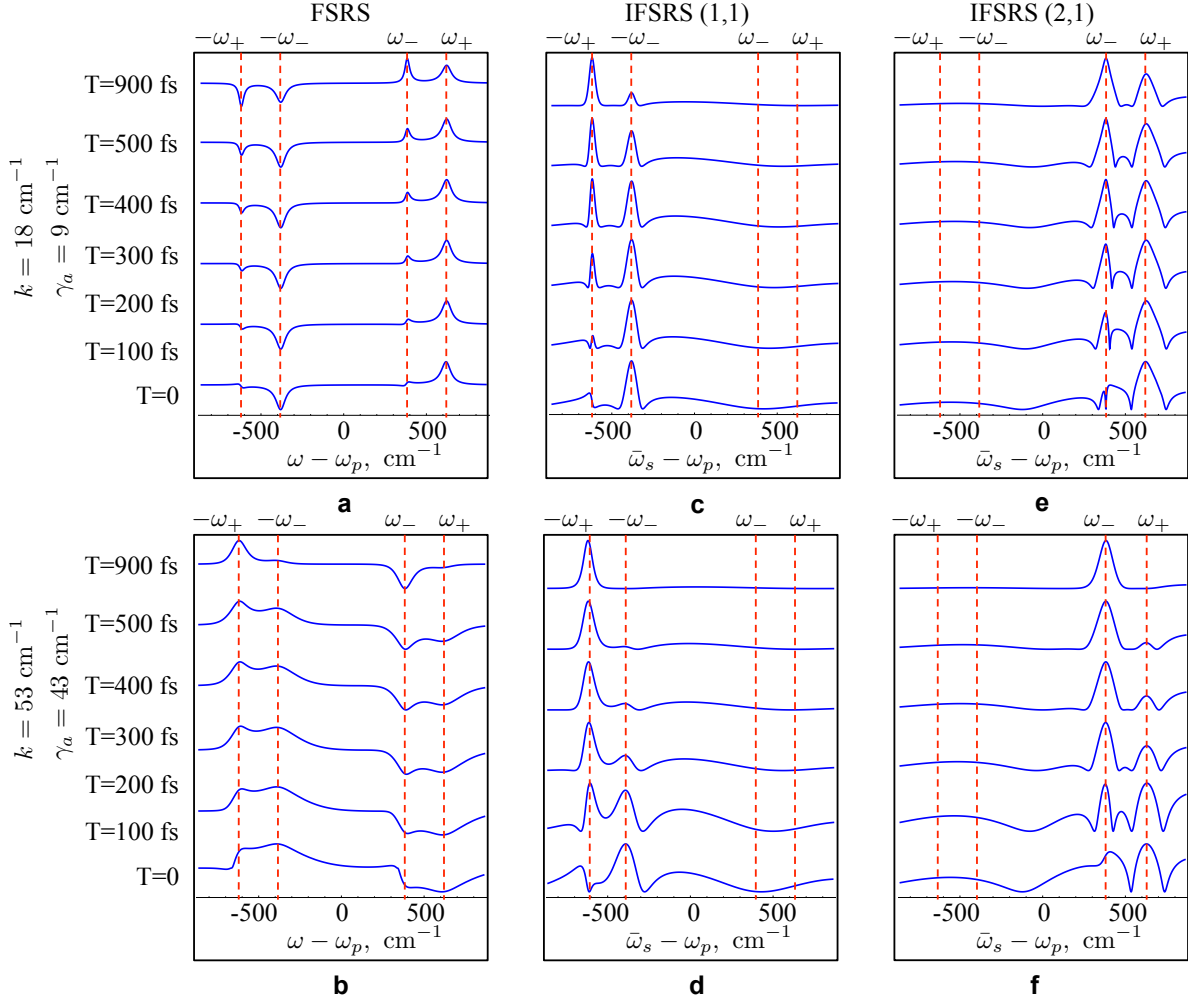


Figure 5: (Color online) First column: **a** - series of the snapshots using classical FSRS signal (??) for a time evolving vibrational mode i vs $\omega - \omega_p$ for slow tunneling rate $k = 18 \text{ cm}^{-1}$ and narrow dephasing $\gamma_a = 9 \text{ cm}^{-1}$, **b** - same as **a** but for fast tunneling rate $k = 53 \text{ cm}^{-1}$ and broad dephasing $\gamma_a = 43 \text{ cm}^{-1}$. Second column: **c**, **d** - same as **a**, **b** but for $S_{IFSRS}^{(1,1)}$ in Eq. (??). Third column: **e** and **f** - same as **a**, **b** but for $S_{IFSRS}^{(2,1)}$ given by Eq. (??) vs $\bar{\omega}_s - \omega_p$. All parameters are the same as in Fig. 3.

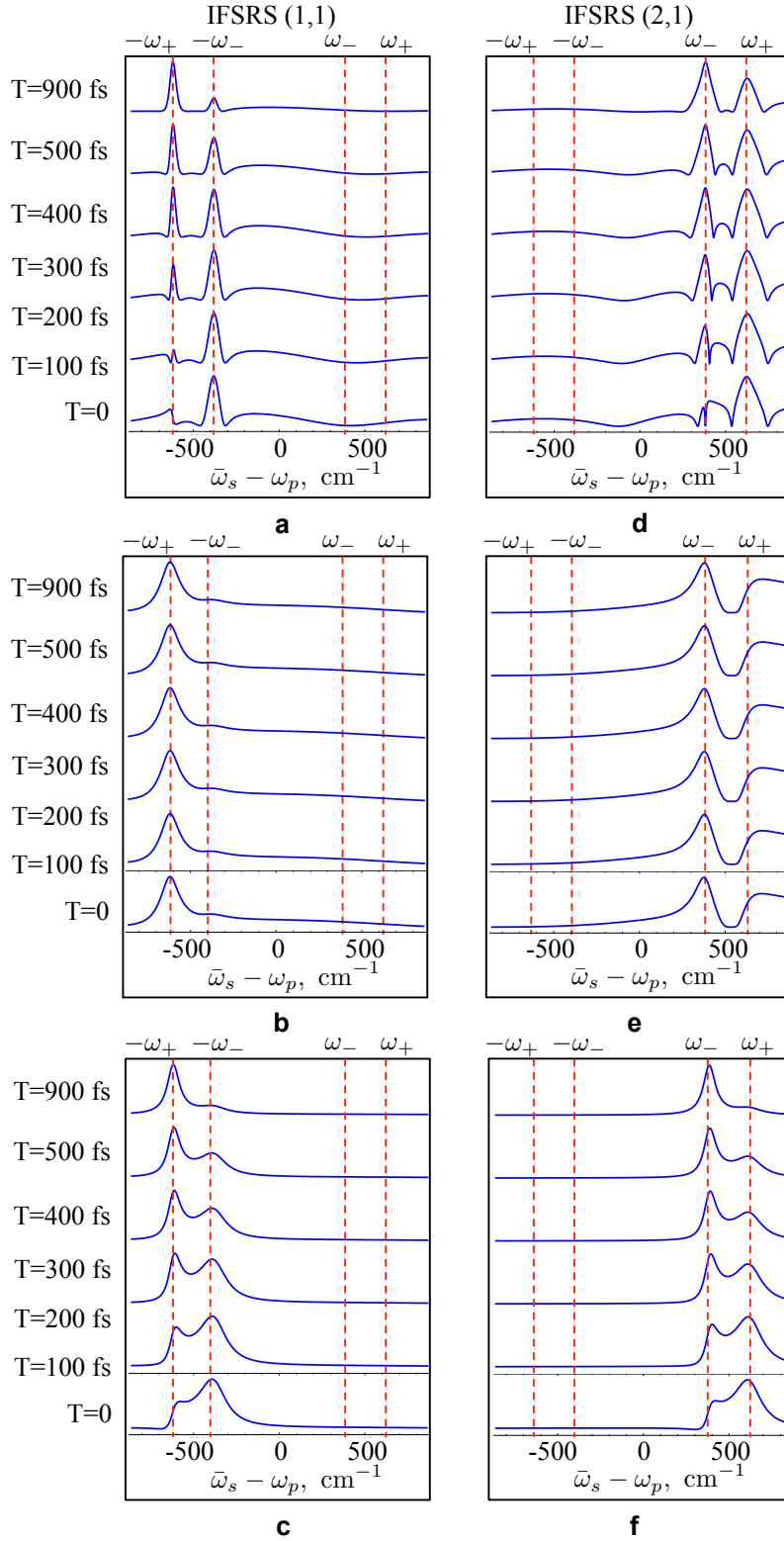


Figure 6: (Color online) Left column: Series of the snapshots using $S_{IFSRS}^{(1,1)}$ signal (??) vs $\bar{\omega}_s - \omega_p$ for entangled state (??) - **a**, correlated - **b** and uncorrelated - **c** separable states. **d**, **e**, and **f** - same as **a**, **b**, and **c** but for $S_{IFSRS}^{(2,1)}$ signal (??). All parameters are the same as in Fig. 3.